The hard X-ray emission from the Vela Pulsar Wind Nebula

V. Mangano [a] F. Bocchino [b] G. Cusumano [a] E. Massaro [c,d] T. Mineo [a]

[a] *Istituto di Astrofisica Spaziale e Fisica Cosmica - Sezione di Palermo, INAF-CNR, Via Ugo La Malfa 153, I-90146 Palermo, Italy*

[b] *Osservatorio Astronomico di Palermo, Piazza dei Normanni 1, I-90100 Palermo, Italy*

[c] *Dipartimento di Fisica, Universitá La Sapienza, Piazzale A. Moro 2, I-00185 Roma, Italy*

[d] *Istituto di Astrofisica Spaziale e Fisica Cosmica - Sezione di Roma, INAF-CNR, Via del Fosso del cavaliere 100, I-00113 Roma, Italy*

Abstract

We present the results of a preliminary spectral analysis performed on the BeppoSAX and XMM observations of the Vela plerion. The broad energy range covered by the instruments on board the two observatories allows an evaluation of the spectral parameters of the high energy emission model and provides an indication on the morphology of the source emission above 10 keV. We confirm the softening of the PWN spectrum (3–10 keV band) at distances greater than $4'$ from the pulsar and estimate the diameter of the high energy (> 10 keV) emission region to be on the order of $25'$–$30'$.

Key words: Supernova Remnants, Pulsar Wind Nebulae, X–rays

1 Introduction

Plerion emission is observed across the entire electromagnetic spectrum, but in the hard-X/soft-γ rays very little is known about the spectra of plerions. The Vela SNR is one of the nearest plerions, its distance is estimated to be about 300 pc (Dodson et al. 2003); thus its structure can be studied in detail. Chandra observations provided very detailed X–ray images of the source in the 0.1-10 keV band, showing the presence of a compact nebula, a jet-counterjet originating from the pulsar and a double bow structure (Helfand et al. 2001,

Pavlov et al. 2001a) extending in a region smaller than $0'.7$ around the pulsar. Kargaltsev and Pavlov (2004) presented maps of the 2-10 keV photon index ($F(E_\gamma) \propto E_\gamma^{-\Gamma}$) with resolutions of $2''.5$ and $10''$ which show how the emission is harder ($\Gamma \simeq 1.2$–1.4) in the near surroundings of the pulsar (less than $1'$) and becomes softer ($\Gamma \simeq 1.6$–1.8) at distances of $2'$–$3'$. Mori et al. (2003) analysing PN data from a recent XMM observation extracted a circular region around the pulsar position within a radius of $1'$ and modelled the spectral PWN emission with a power law of spectral index of 1.64 ± 0.08. The present knowledge about the hard X–ray emission from the Vela SNR is rather poor. The most recent data are those obtained in the energy range 60–400 keV with OSSE–CGRO (FOV $3°.8 \times 11°.4$) (De Jager, Strickman & Harding 1996): a single power law fit indicated a quite hard spectrum but with the uncertain photon index Γ of 1.6 ± 0.5. This result was found consistent with previous finding obtained with the Birmingham Spacelab 2 coded mask detector (2-25 keV) (Willmore et al. 1992), that gave $\Gamma = 1.74 \pm 0.08$ for a radius of $6'$–$7'$.

We will present a preliminar spectral analysis of BeppoSAX and XMM archival observations of PSR 0833-45 aiming at extracting as much information as possible about the Vela PWN emission in the 3-200 energy range.

2 BeppoSAX and XMM observations and data reduction

The XMM-Newton observation used for the present analysis was performed on 1 December 2000 with an exposure of 38 ks. MOS1 operated in Large Window mode and MOS2 in Small Window mode. We reduced the EPIC MOS1 data with the XMM Science Analysis Software (SAS) version 6.0 and performed standard screening of EPIC data. A complete image of the source extracted from MOS1 data is available from the center to $2'.5$ and from $5'.5$ to $14'$ (Fig. 1). The MOS2 data were not taken into account because of an even smaller central active part of the detector. A second XMM-Newton of the Vela pulsar was perfromed on 2 December 2000, but we did not use it for our preliminar analysis because it suffered high background contamination. Spectra were extracted from circular regions with different radii, always contained in the central square region of Fig. 1. The background spectrum for MOS1 was extracted from instrumental and particle background maps obtained by XMM observations with the filter wheel in the 'closed' position (Marty et al. 2002). According to De Luca & Molendi (2004), the cosmic X–ray background contribution in the selected regions is negligible with respect to the instrumental background. The spectral response matrix and effective area were computed for each region using the SAS tasks *rmfgen* and *arfgen* respectively with the standard recipe for extended sources.

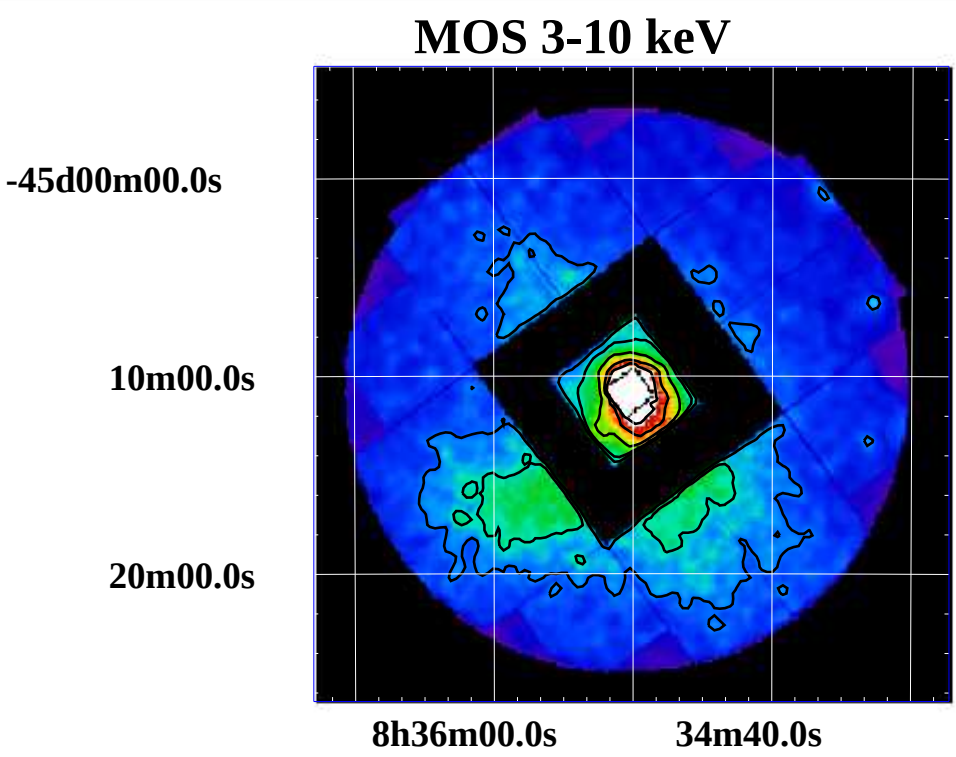

Fig. 1. XMM–MOS1 image of the Vela PWN in the 3–10 keV band. Contour levels are at 5×10^{-4}, 1×10^{-3}, 2×10^{-3} and 8×10^{-3} times the brightest point in the image respectively.

The BeppoSAX observation of the Vela pulsar region was performed on 18–20 November 1997 for a total net exposure of 84 ks in the MECS (1.7–10 keV) and 38 ks in the PDS (15–300 keV) Standard procedures and selection criteria were applied to the data using the SAXDAS v.2.0.0. package. PDS spectrum includes all the plerion emission (1°.3 FOV). MECS spectra were extracted from a set of circular regions centered on PSR 0833-45, starting form a 4′ radius. For the spectral analysis of the MECS data a suitable auxiliary matrix was created to correct for the vignetting whose influence becomes relevant for source with an extension greater than 4′. The background spectrum of the MECS was extracted from archival blank fields, while in the PDS it is simultaneously monitored by the rocking mode of the collimator. For both BeppoSAX/MECS and XMM/MOS, only events with an energy higher than 3 keV were selected for the spectral analysis so as to exclude the soft thermal contribution from the pulsar (Pavlov et al. 2001b). The uncertainties reported in the following are at 1 standard deviation for one interesting parameter.

3 Spectral analysis

We first fitted all the extracted XMM/MOS and BeppoSAX/MECS and PDS spectra with a simple power law model ($F(E) = K(E/1\ \mathrm{keV})^{-\Gamma}$). All the fits were good, with χ^2_r spanning from 1.1(94dof) to 1.01(177dof) for MOS1, χ^2_r in the range 0.93-1.02 (66dof) for MECS and $\chi^2_r \sim 0.73(16dof)$ for PDS. A plot of the MOS and MECS photon index as a function of the extraction radius is shown in Fig. 2. The value of Γ changes with the extraction radius: for a radius $\leq 2'$ it is in the range 1.53–1.57, in agreement with Kargaltsev and Pavlov (2004), while for higher radii it increases to 1.67, in agreement with the value reported by Willmore et al. (1992), indicating a quite mild softening of the spectrum in the outer region of the plerion. The PDS spectrum in the 15–200 keV energy range has a photon index equal to 2.00±0.05, significantly higher than those found in the lower energy range. This indicates that a spectral steepening occurs at higher energies. Furthermore, it is also higher than the value obtained with OSSE (De Jager et al. 1996), although statistically compatible because of the large uncertainty in their photon index estimate.

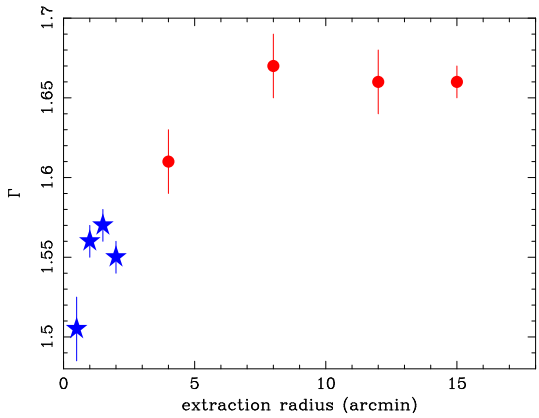

Fig. 2. Power law index of MOS (stars) and MECS (filled circles) spectra at varying extraction radius.

Moreover, we evaluated combined fits of MECS–PDS and of MOS–PDS spectra using two different spectral laws: a simple power law and a continuous steepening law, characterized by a linear dependence of the spectral slope upon the logarithm of energy:

$$F(E) = K_{log}(E/1\ \mathrm{keV})^{-(\alpha+\beta\ Log\ (E/1\ \mathrm{keV}))} \quad (1)$$

This law is often used to model spectra that are continuously steepening with energy (Massaro et al 2000). In the simultaneous fit an intercalibration factor (f_{MP}) was included to take into account the systematics between the two instruments. From in–flight calibration we expect an f_{MP} value between 0.77

and 0.93 when the emission region observed in the PDS is fully selected in the MECS/MOS image (Fiore et al. 1999, Kirsch et al 2004). The simple power law model can be rejected for all extraction regions in the MECS and in the MOS because of the high χ^2_r values (see Table 1). Furthermore, residuals in the PDS range show large systematic deviations for any extraction radius (Fig. 3, left panel and Table 1, last column). The log-parabolic law (Eq. (1)) gave acceptable fits for all extraction radii (see Table 2) and the f_{MP} resulted in agreement with the expected range for radii $\geq 12'$. This result is an indication that to fully select the 3–10 keV emission corresponding to the 15–200 keV emission observed in the FoV of the PDS, we must extract photons in a region with a radius of about $12'$–$15'$. The $15'$ MECS and PDS spectra are shown in Fig. 3.

Table 1
Best–fit model parameters of MOS–PDS and MECS–PDS energy spectra with a single power law. The normalization K is expressed in units of 10^{-2} photons cm^{-2} s^{-1} keV^{-1} at 1 keV. Given the different statistical content between MOS/MECS and PDS spectra we report also χ^2_r values relative to PDS data only (last column in the table).

Inst	Radius	Γ	K	f_{MP}	χ^2_r (d.o.f.)	$\chi^2_{r,pds}$ (d.o.f.)
MOS	$0'.5$	1.687±0.024	0.52±0.02	3.56±0.17	1.83 (111)	4.60 (15)
MOS	$1'$	1.650±0.017	1.09±0.03	1.49±0.05	1.44 (171)	5.61 (15)
MOS	$1'.5$	1.645±0.017	1.24±0.03	1.29±0.05	1.51 (185)	5.75 (15)
MOS	$2'$	1.641±0.016	1.34±0.03	1.17±0.04	1.46 (194)	5.90 (15)
MECS	$4'$	1.667±0.016	1.65±0.04	1.04±0.03	1.84 (83)	5.15 (15)
MECS	$8'$	1.712±0.015	2.01±0.05	0.99±0.03	1.55 (83)	3.99 (15)
MECS	$12'$	1.707±0.014	2.31±0.05	0.85±0.03	1.64 (83)	4.11 (15)
MECS	$15'$	1.701±0.014	2.79±0.06	0.69±0.02	1.67 (83)	4.24 (15)

Table 2
Best–fit model parameters of MOS–PDS and MECS–PDS energy spectra with the log-parabolic law (Eq. (1)). The normalization K_{log} is expressed in units of 10^{-2} photons cm^{-2} s^{-1} keV^{-1} at 1 keV. Given the different statistical content between MOS/MECS and PDS spectra we report also χ^2_r values relative to PDS data only (last column in the table).

Inst	Radius	α	β	K_{log}	f_{MP}	χ^2_r (d.o.f.)	$\chi^2_{r,pds}$ (d.o.f.)
MOS/PDS	$0'.5$	1.13±0.06	-0.29±0.03	0.30±0.03	3.98±0.20	1.04 (110)	0.77 (14)
MOS/PDS	$1'$	1.22±0.05	-0.26±0.03	0.74±0.04	1.85±0.08	0.92 (170)	0.76 (14)
MOS/PDS	$1'.5$	1.22±0.05	-0.26±0.03	0.85±0.04	1.63±0.07	1.01 (184)	0.76 (14)
MOS/PDS	$2'$	1.21±0.05	-0.27±0.03	0.92±0.04	1.50±0.07	0.96 (193)	0.76 (14)
MECS/PDS	$4'$	1.24±0.05	-0.26±0.03	1.12±0.05	1.29±0.05	0.84 (82)	0.76 (14)
MECS/PDS	$8'$	1.36±0.05	-0.22±0.03	1.48±0.07	1.20±0.05	0.84 (82)	0.75 (14)
MECS/PDS	$12'$	1.36±0.05	-0.22±0.03	1.70±0.08	1.03±0.04	0.91 (82)	0.75 (14)
MECS/PDS	$15'$	1.36±0.05	-0.21±0.03	2.08±0.10	0.84±0.03	0.98 (82)	0.76 (14)

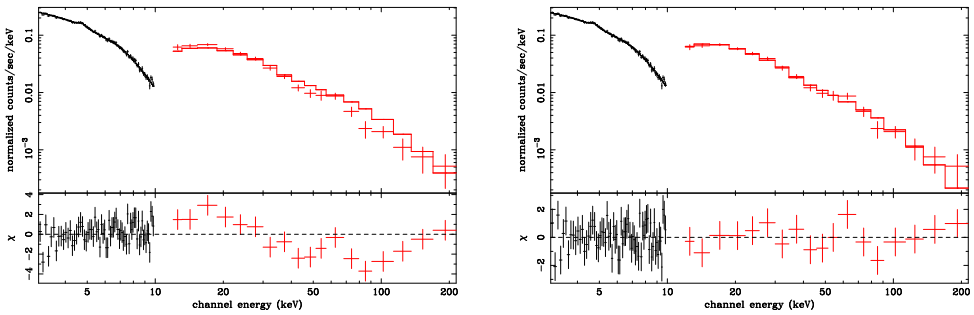

Fig. 3. Best fit of MECS (15′ extraction radius) and PDS data with a single power law (left panel) and the log–parabolic law (right panel).

4 Conclusions

The extended emission of the Vela PWN in the 3–10 keV band that we can see in Fig. 1 softens at growing distances from the pulsar: the photon index value passes from 1.50±0.02 to 1.66±0.01 as the radius increases from 0′.5 to 15′. High energy emission from the source, detected by the PDS (15–200 keV), originates from an extended region around the pulsar too. The photon index of the PDS spectrum in the 15–200 keV band is 2.00±0.05 indicating a spectral steepening at higher energies. The 3–200 keV spectrum of the PWN is well fitted by a log–parabolic law. Since the best fit value of the intercalibration factor derived from the simultaneous fit to MOS/MECS and PDS is compatible with the expected range (Section 3) only for an extraction radius of MECS data greater than 12′, we conclude that the hard X–ray emission of the Vela PWN is likely coming from a region of 12′–15′ radius around the pulsar.

References

De Jager O.C., Harding A.K., Strickman M.S. OSSE Detection of Gamma Rays from the VELA Synchrotron Nebula ApJ 460, 729-734, 1996

De Luca, A. & Molendi, S. The 2-8 keV cosmic X-ray background spectrum as observed with XMM-Newton A&A, 419, 837-848, 2004

Dodson R., Legge, D., Reynolds J.E., McCulloch, P.M. The Vela Pulsar's Proper Motion and Parallax Derived from VLBI Observations ApJ 596, 1137-1141, 2003

Fiore F., Guainazzi M., Grandi P. et al. in Cookbook for BeppoSAX NFI Spectral Analysis, BeppoSAX Science Data Center, version 1.2, 1999, http://www.asdc.asi.it/

Helfand D.J., Gotthelf E.V., Halpern J.P. Vela Pulsar and Its Synchrotron Nebula ApJ 556, 380-391, 2001

Kargaltsev O.Y., Pavlov G. Spatially Resolved Spectrum of the Vela PWN in Young Neutron Stars and Their Environments, IAU Symp. 218, F. Camilo and B.M. Gaensler eds., p. 195-198, 2004

Kirsh M.G.F, Altieri B., Chen B. et al. XMM Newton (cross) calibration, XMM-

SOC-CAL-TN-0055, 2004,
http://xmm.vilspa.esa.es/external/xmm_sw_cal/calib/index.shtml

Marty, P.B., Kneib, J.-P., Sadat, R. et al. Data analysis method for XMM-Newton observations of extended sources and application to bright massive clusters of galaxies at z=0.2 proc. SPIE. vol 4851, pp 208-222, 2002

Massaro, E., Cusumano, G., Litterio, M., Mineo, T. Fine phase resolved spectroscopy of the X-ray emission of the Crab pulsar (PSR B0531+21) observed with BeppoSAX A&A 361, 695-703, 2000

Mori K., Hailey C.J., Paerels F., Zane S. XMM-Newton Observations of the Vela Pulsar AdvSpRes 33-39, 503-506, 2004

Pavlov G.G., Kargaltsev O.Y., Sanwal, D., Garmire, G.P. Variability of the Vela Pulsar Wind Nebula Observed with Chandra ApJ 554, L189-192, 2001a

Pavlov G.G., Zavlin V.E., Sanwal, D. et al. The X-Ray Spectrum of the Vela Pulsar Resolved with the Chandra X-Ray Observatory ApJ 552, L129-133, 2001b

Willmore A.P., Eyles C.J., Skinner, G.K., Watt, M.P. Hard X-ray emission from the VELA supernova remnant MNRAS 254, 139-145, 1992